LETTER

doi:10.1038/nature11720

Controlling dielectrics with the electric field of light

Martin Schultze[1,2], Elisabeth M. Bothschafter[1,3], Annkatrin Sommer[1], Simon Holzner[1], Wolfgang Schweinberger[1], Markus Fiess[1], Michael Hofstetter[2], Reinhard Kienberger[1,3], Vadym Apalkov[4], Vladislav S. Yakovlev[2], Mark I. Stockman[4] & Ferenc Krausz[1,2]

The control of the electric and optical properties of semiconductors with microwave fields forms the basis of modern electronics, information processing and optical communications. The extension of such control to optical frequencies calls for wideband materials such as dielectrics, which require strong electric fields to alter their physical properties[1–5]. Few-cycle laser pulses permit damage-free exposure of dielectrics to electric fields of several volts per ångström[6] and significant modifications in their electronic system[6–13]. Fields of such strength and temporal confinement can turn a dielectric from an insulating state to a conducting state within the optical period[14]. However, to extend electric signal control and processing to light frequencies depends on the feasibility of reversing these effects approximately as fast as they can be induced. Here we study the underlying electron processes with sub-femtosecond solid-state spectroscopy, which reveals the feasibility of manipulating the electronic structure and electric polarizability of a dielectric reversibly with the electric field of light. We irradiate a dielectric (fused silica) with a waveform-controlled near-infrared few-cycle light field of several volts per angström and probe changes in extreme-ultraviolet absorptivity and near-infrared reflectivity on a timescale of approximately a hundred attoseconds to a few femtoseconds. The field-induced changes follow, in a highly nonlinear fashion, the turn-on and turn-off behaviour of the driving field, in agreement with the predictions of a quantum mechanical model. The ultrafast reversibility of the effects implies that the physical properties of a dielectric can be controlled with the electric field of light, offering the potential for petahertz-bandwidth signal manipulation.

A dielectric subjected to a weak optical field reacts to its change instantly (adiabatically) as long as the laser frequency $\omega_L \ll \Delta_{gap}/\hbar$, where Δ_{gap} is the gap between the valence band and conduction band; for silica $\Delta_{gap} \approx 9$ eV (numerical values below are given for this material). When the strength of the electric field F approaches the critical field strength, inducing a change in electron potential energy by Δ_{gap} over the lattice period $a \approx 5$ Å then

$$F_{crit} = \frac{\Delta_{gap}}{|e|a} \approx 2\,\mathrm{V\,\AA^{-1}} \quad (1)$$

(where e is the electron charge), and Zener-type transitions[1] inject electrons into the entire conduction band within its spectral width $\Delta_c \approx 10$ eV. This by itself, irrespective of ω_L, leads to ultrafast dynamics of the induced broadband polarization on a timescale of $\hbar/\Delta_c \approx 0.1$ fs. Hence, real-time access to strong-field-induced dynamics in dielectrics calls for sub-femtosecond temporal resolution. In our work, this was provided by the envelope of sub-100-attosecond extreme-ultraviolet (XUV) pulses and the controlled instantaneous field of few-femtosecond near-infrared (NIR) laser pulses.

In a first set of experiments, the waveform-controlled linearly polarized field, $F_L(t)$, of NIR laser pulses of less than 4 fs (carrier wavelength $\lambda_L = 780$ nm and wave cycle $T_L = 2\pi/\omega_L = 2.6$ fs), along with isolated 72-as XUV pulses carried at $\hbar\omega_{XUV} \approx 105$ eV and polarized parallel to the laser field, impinged collinearly on a free-standing 125-nm SiO_2 film (see Fig. 1a and Methods). The XUV pulse probed the processes induced by $F_L(t)$ by promoting electrons from the L-shell of silicon into the conduction band states. Transient changes in the conduction band are reflected in the XUV spectra recorded as a function of delay of the XUV probe with respect to the NIR-field excitation; see Fig. 1c. We note that the XUV pulse induces polarization over the entire band $\Delta_c/\hbar$, which largely dephases within $\tau_{dephasing} \sim \hbar/\Delta_c \sim 100$ as after passage of the XUV pulse through the sample. The XUV light radiated from the sample coherently with the XUV probe field therefore decayed within about 100 as after the XUV pulse. This permitted—in contrast with previous experiments in atomic gases[15]—us to record attosecond transient absorption spectra that provide information about the evolving state of the quantum system at the instant of probing and are not appreciably affected by the ongoing strong-field excitation afterwards.

We supplemented attosecond probing with simultaneous streaking[16] of the excitation field $F_L(t)$ (Fig. 1b) in a neon gas jet in front of the SiO_2 sample. Figure 1a displays the laser field and the XUV pulse envelope retrieved from this measurement. Simultaneous implementation of these two attosecond techniques permitted assignment of the transient absorption spectra to well-defined moments within the excitation field, $F_L(t)$, providing absolute timing of the processes under scrutiny.

For a detailed analysis, we evaluate the absorbance A, given by $A(\hbar\omega_{XUV}) = \alpha(\hbar\omega_{XUV})d$, where $\alpha(\hbar\omega_{XUV})$ is the absorption coefficient at the photon energy $\hbar\omega_{XUV}$, and d is the thickness of the sample. We first discuss XUV absorption near the edge of the conduction band. The solid line in Fig. 2b shows the transient change in A induced by the NIR field plotted in Fig. 2a; its measured peak electric field strength is $F_0 = 2.5 \pm 0.5$ V Å^{-1}. It reveals a large (>10%) increase of the sample's XUV transmittance over sub-femtosecond intervals. The oscillations in absorbance at a frequency of $2\omega_L$ are accompanied by similar oscillations in the position of the conduction-band edge (Fig. 2c). The measurement resolves condensed-matter processes driven by the instantaneous field of visible light. The changes emerge within a single half-cycle of the driving field and terminate with similar abruptness several femtoseconds later; see also the inset of Fig. 2b. The XUV absorption bleaching extends, with similar temporal behaviour, over the entire conduction band; see Supplementary Fig. 1.

To analyse the observed field-induced modifications, we adapted—with exactly the same parameters—the quantum-mechanical model developed for describing electric currents in dielectrics induced by strong, few-cycle NIR fields under physical conditions identical to the experiments of this work[14]. Briefly, it is based on the time-dependent Schrödinger equation in the presence of the measured field $F_L(t)$, incorporating field screening but neglecting electron collisions and excitonic effects. For a detailed description, see Supplementary Information. The model accurately predicts the magnitude and the sub-femtosecond temporal structure of the observed modulation in strength (Fig. 2b) and position (Fig. 2c) of the 109-eV absorption line, as well as the bandwidth and the strength of the XUV absorption bleaching (Supplementary Fig. 1). Agreement in the phase of these modulations with respect to the oscillating laser field (Fig. 2b, c)

[1]Max-Planck-Institut für Quantenoptik, Hans-Kopfermann-Strasse 1, D-85748 Garching, Germany. [2]Fakultät für Physik, Ludwig-Maximilians-Universität, Geschwister-Scholl-Platz 1, D-80539 München, Germany. [3]Physik-Department, Technische Universität München, James-Franck-Strasse, D-85748 Garching, Germany. [4]Department of Physics, Georgia State University, Atlanta, Georgia 30340, USA.

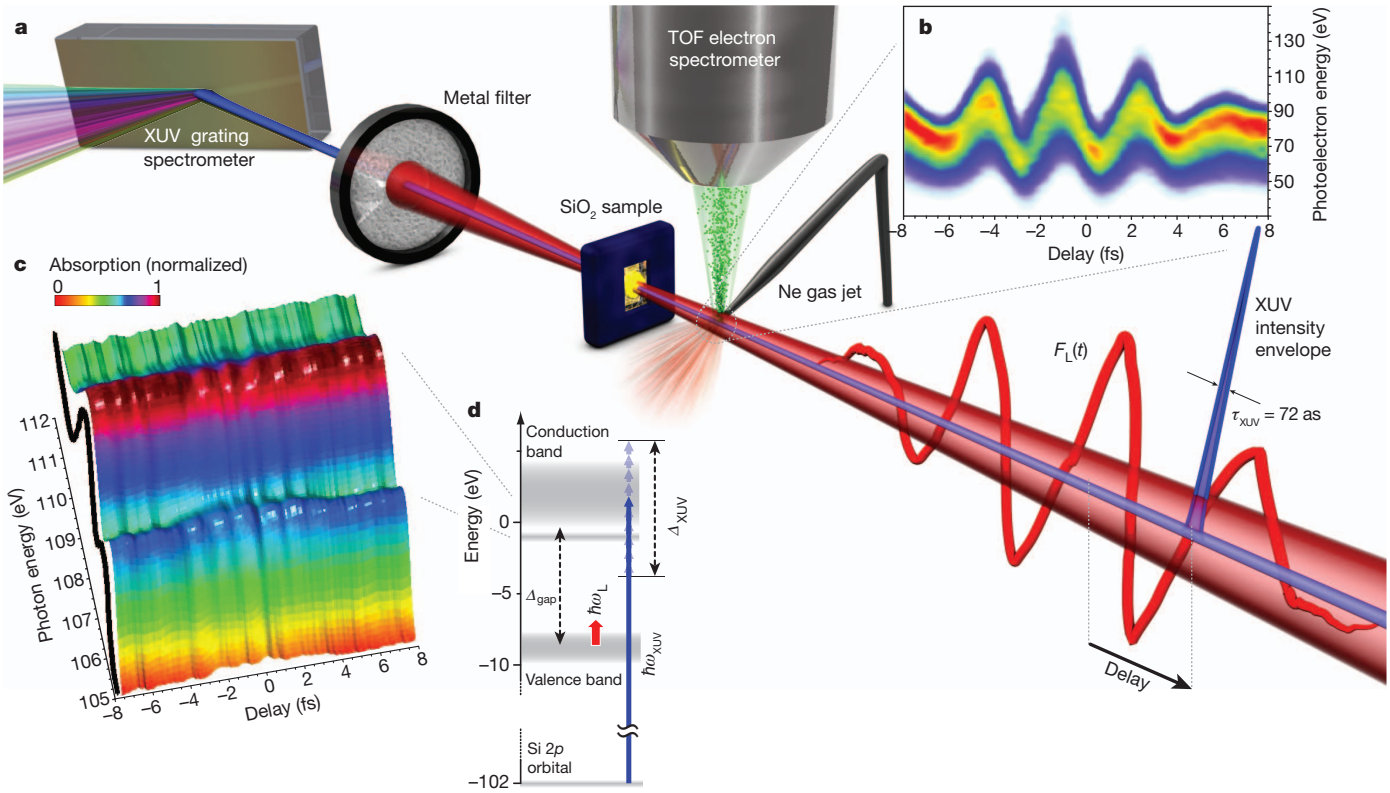

Figure 1 | Simultaneous attosecond absorption and streaking spectroscopy. **a**, Schematic illustration of the experimental set-up. TOF, time of flight. **b**, Attosecond streaking spectrogram of the 72-attosecond (full-width at half maximum) isolated XUV pulse and a near-single-cycle NIR pulse used in the experiments. The spectrogram was recorded by measuring the energy spectrum of photoelectrons released by the XUV pulse into the NIR field as a function of NIR–XUV delay. **c**, Attosecond transient absorption spectrogram of a 125-nm-thick SiO_2 membrane in the range 105–112 eV as a function of delay between the sub-100-attosecond XUV pulse and the NIR laser pulse with a delay step of $\Delta t_{delay} = 100$ as (the black line shows the synchrotron-XANES absorption data[24] for comparison). **d**, Schematic energy level diagram of SiO_2. The blue arrow represents the XUV absorption from Si L-states to the SiO_2 conduction band. The 9-eV bandgap between valence and conduction band exceeds the NIR photon energy by a factor of 6, as indicated by the red arrow.

supports our understanding that it is the instantaneous field that drives the processes.

In a second set of experiments, we scrutinized the influence of the strong field on the polarizability in the NIR range by studying the transmitted and reflected NIR light (for details, see Methods and Supplementary Information). Within our experimental accuracy of about $\pm 1.2\%$ (dictated by the laser pulse-to-pulse stability), the transmittance of our NIR beam did not vary up to the intensity threshold for breakdown. In contrast, the power of the reflected beam, detected in a *z*-scan geometry, increased by nearly an order of magnitude for field strengths approaching the breakdown threshold as shown in Fig. 3a. To ensure the highest contrast for the subsequent pump–probe study (see below), this measurement was implemented with

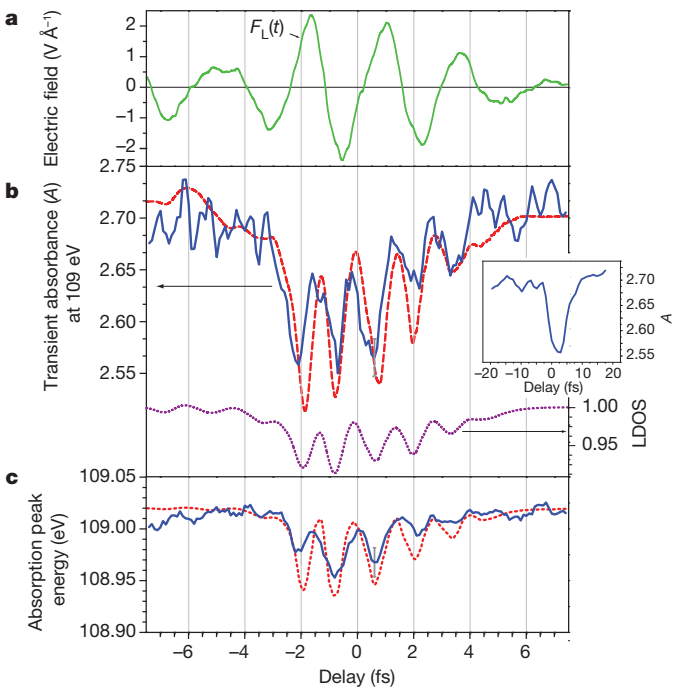

Figure 2 | Attosecond time-resolved strong-field-induced effects in SiO_2. Solid lines are experimental results; dashed lines are predictions of theoretical modelling. **a**, Electric field of the few-cycle NIR laser pulse impinging on the SiO_2 sample, $F_L(t)$, as extracted from attosecond streaking (see Fig. 1b). **b**, Transient change of the absorbance $A(\hbar\omega_{XUV}) = \alpha(\hbar\omega_{XUV})d$ integrated over a 1-eV bandwidth at $\hbar\omega = 109$ eV, as a function of the delay (the delay step is $\Delta t_{delay} = 100$ as) between the 72-as XUV probe and the NIR laser pulse (blue solid line), along with the prediction of our quantum mechanical model (red dashed line). The inset shows the evolution of *A* in a more extended delay range, recorded with larger delay steps ($\Delta t_{delay} = 0.5$ fs). The error bar in **b** represents the standard error of the average over 15 spectral lineouts within the energy range 108.5–109.5 eV; it exhibits little variation over the delay scan. The dashed violet line is the calculated local density of states (LDOS) at the position of a Si atom (integrated over the energy range accessed by the XUV pulse, for more details, see Supplementary Information) versus delay of the XUV probe. **c**, Energy of the absorption peak at 109 eV subject to an optical-field-induced (dynamic Stark) shift (the blue solid line shows the measurement, the red dashed line shows the calculation). The error bar in **c** represents the 95% confidence interval of the peak position of a least-squares fit of the area of a Gaussian function to the area under the absorption line; it exhibits little variation over the delay scan.

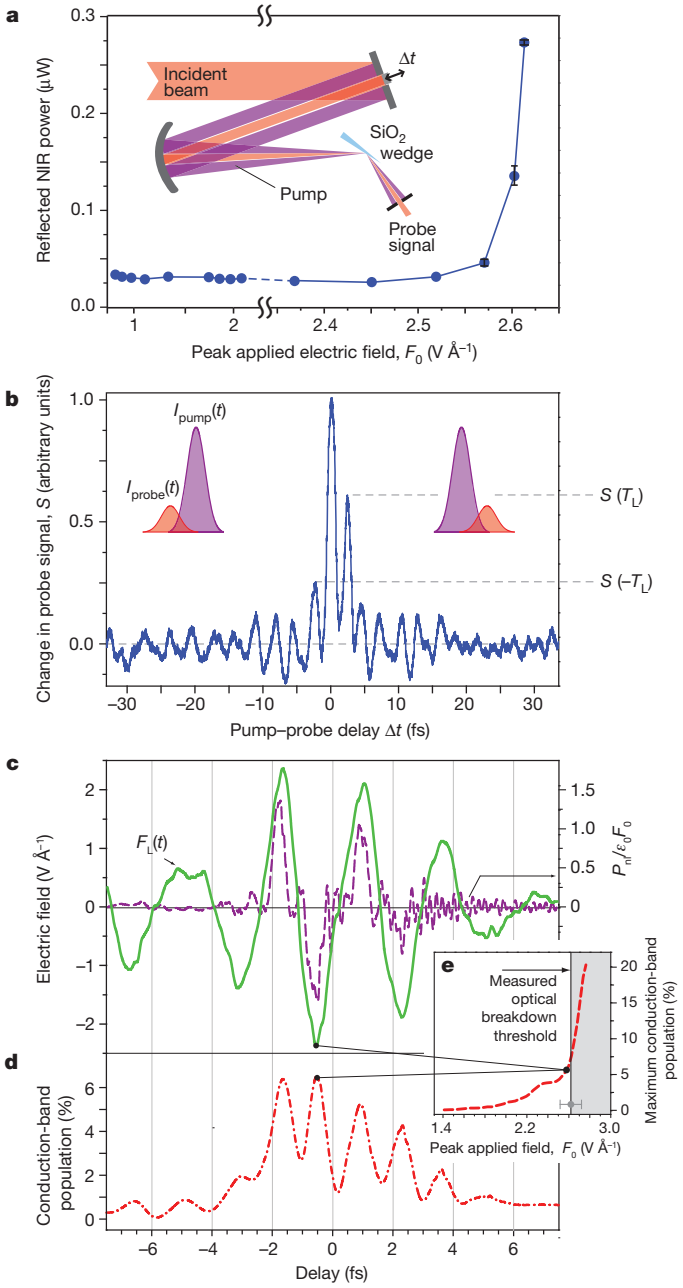

Figure 3 | Wave-cycle-resolved NIR femtosecond probing of strong-field-induced nonlinear reflectivity of SiO_2. **a**, Reflected power of *p*-polarized NIR laser pulses of less than 4 fs incident at Brewster's angle on the thin-wedged sample of fused silica as a function of peak electric field (penetrating into the sample). The process is fully reversible for several thousand laser shots before irreversible damage occurs owing to self-focusing inside the sample rather than on the surface. The data points are averaged over 3,000 laser pulses (error bars represent the standard deviation). Inset, schematic illustration of the pump–probe transient reflectivity set-up (for description, see Methods). **b**, Reflected power on axis of the probe pulse of less than 4 fs (represented by the red beam; intensity envelope I_{probe}) as a function of the delay with respect to the strong pump pulse of less than 4 fs (illustrated by the violet beam; intensity envelope I_{pump}). The curve is the result of an average of ten scans; for representative individual scans and details, see Supplementary Fig. 2 and the related description in the Supplementary Information. The reflected probe signal at delays of $\Delta t = \pm T_L$ is denoted by $S(\pm T_L)$. **c**, Electric field of the few-cycle NIR laser pulse impinging on the SiO_2 sample, $F_L(t)$, as extracted from attosecond streaking (see green solid line in Fig. 1b), and the resulting nonlinear polarization $P_{nl}(t)$, normalized to $\varepsilon_0 F_0$, predicted by our model (purple dashed line). **d**, Computed transient evolution of the population of (unperturbed) conduction band states timed to the laser field. **e**, Peak transient conduction band population versus peak applied field strength. The grey shading represents the experimental value of the optical breakdown threshold, as determined from the reflectance measurement yielding the data shown in **a**.

light impinging at Brewster's angle and polarized in the plane of incidence (*p*-polarized). The dependence on the field strength was extremely nonlinear, closely resembling that of the field-induced current[14]. Our model is not yet applicable to an oblique angle of incidence but did correctly predict the field-strength-dependence of the current[14]. The similarity in the intensity scaling of the optical current and reflectivity points to their common physical origin: the field-enhanced polarizability.

Is this effect mainly due to a conduction-band population surviving the few-cycle field or to reversible effects being not only turned on but also turned off by the field? Although the XUV bleaching already suggests that the latter is more likely, we sought additional evidence using time-resolved optical reflectometry. To this end, we split the incident pulse into a strong pump and a weak probe beam, with the sum of the two field maxima being slightly below the breakdown threshold, and measured the reflected probe intensity as a function of the delay Δt; see the sketch of the apparatus in Fig. 3a and the result in Fig. 3b.

Comparing the reflected probe signal S at delays $\Delta t = \pm T_L$, we found the signal to be significantly greater in the immediate aftermath of the strong pulse, $S(T_L)/S(-T_L) = 2.1 \pm 0.2$ (with no measurable dependence on the carrier-envelope phase to within the measurement accuracy limited by intensity fluctuations). However, comparing signals on opposite fringe peaks at $\Delta t \approx \pm 2T_L$, $\pm 3T_L$,..., showed no appreciable asymmetry—$S(nT_L) \approx S(-nT_L)$, $n > 1$—within our experimental precision. If a significant fraction of the induced nonlinear reflectivity (and, consequently, polarization) survived the pulse peak over several cycles, this would imply $S(nT_L)$ significantly larger than $S(-nT_L)$, owing to a much larger fraction of the probe pulse experiencing the increased reflectivity. Our observation thus provides compelling evidence, in a model-independent manner, for the substantial reversibility of the strong-field-induced increase in polarizability on the timescale of the optical wave cycle.

Figure 3c contrasts the applied electric field $F_L(t)$ (solid line) with the calculated field-induced nonlinear polarization $P_{nl}(t)$ normalized to $\varepsilon_0 F_0$ (dashed line). The strongly sharpened half cycles of $P_{nl}(t)$ point to an extremely nonlinear scaling with driving field strength, consistent with the data in Fig. 3a. The nonlinear response is largely confined to the central laser cycle and disappears completely before the end of the pulse. This effect is accompanied by a field-induced transient population and subsequent depopulation of the conduction band, confined, again, to several femtoseconds (see Fig. 3d). For field strengths beyond $F_0 \approx 2.5\ \mathrm{V\,Å^{-1}}$, Fig. 3e shows a near-exponential growth of conduction band population, causing breakdown. In fact, the maximum field we could safely apply to our samples before breakdown was $F_0 \approx 2.5\ \mathrm{V\,Å^{-1}}$. Thus, our model also correctly predicts the threshold for optical breakdown (Fig. 3e). Both the nonlinear polarization and the conduction band population induced by the strong field return to near-zero immediately after the laser pulse for $F_0 \leq 2.5\ \mathrm{V\,Å^{-1}}$. This is fully consistent with the abrupt decay of field-induced transient NIR reflectivity and XUV absorption bleaching: see Figs 3b and 2b, respectively. These results imply that the sample exposed to fields as high as $F_0 \leq 2.5\ \mathrm{V\,Å^{-1}}$ resumes its original (field-free) state immediately after exposure. This points towards the reversible, Hamiltonian nature of the laser-induced dynamics up to the critical field strength.

Our quantum mechanical model identifies light-field-induced reversible changes of the local density of states (Fig. 2b), the conduction-band population, and the polarizability as the mechanisms responsible for transient XUV absorption bleaching, NIR reflectivity enhancement, optical breakdown and optical-field-induced currents[14]. The model accounts for all these phenomena with a set of parameters adjusted in ref. 14, which we did not modify in this work. The ability

to predict such a large aggregate of disparate physical effects properly without parameter adjustment provides convincing evidence of the theory's validity.

Considerations presented in ref. 14 provide a hint towards a possible intuitive picture to explain the above effects in terms of the well-known phenomenon of Wannier–Stark localization[17–21]. The field-induced strong transient localization of states is expected to occur in all bands, allowing XUV-induced transitions predominantly between states localized at the same site of the lattice. The energy levels of such colocalized Wannier–Stark states of different bands are shifted identically by the field, leaving the XUV transition energies (between the L-band and conduction band) nearly unchanged. Hence, XUV probing is insensitive to these energy shifts, apart from the small dynamic shifts observed in Fig. 2c, but uncovers dynamic changes in the density of states. The Wannier–Stark ladder formation delivers an intuitive account for the computed decrease of the local density of states (Fig. 2b), which appears to be mainly responsible for the decrease of the XUV absorption. The field-enhanced polarizability of the system can also be related to the strong Stark shifts in the conduction band and valence band: they pull interband transition frequencies into resonance with the visible–NIR spectrum of the driving field[14]. The resultant enhancement in polarizability appears to be the common origin of the optical-field-induced reflectivity observed here and the currents observed in ref. 14. In spite of the consistency of this argument, the intuitive Wannier–Stark picture remains hypothetical until directly verified by experiment, for example, by probing valence band-conduction band transitions with sub-femtosecond resolution.

In conclusion, the synergistic use of attosecond streaking and absorption spectroscopy and wave-cycle-resolved optical reflectivity measurements provide real-time insight into strong-field phenomena in dielectrics on sub-femtosecond to few-femtosecond timescales. The experiments reveal, in agreement with quantum-mechanical modelling, that field-induced changes of all the physical quantities studied are reversible up to the critical field strength, that is, they can be turned on and off on the timescale of the optical period. Controlling the properties of dielectrics with the instantaneous electric field of light points the way towards petahertz signal sampling and processing technologies.

METHODS SUMMARY

XUV transmittivity. Time-resolved XUV absorption spectroscopy was performed with broadband, isolated attosecond XUV pulses generated via high harmonic generation of visible–infrared laser pulses of less than 4 fs (FemtoPower Compact Pro, Femtolasers) in neon. The collinear laser and XUV beam were separated into two arms of a Mach–Zehnder-type interferometer. The relative timing between the two arms could be adjusted with a mirror moved by a piezo translator, and a variable aperture controls the infrared intensity on target. For details, see the Supplementary Information and ref. 22. The XUV and NIR beams were focused with a toroidal mirror on free-standing chemical-vapour-deposited SiO_2 samples (either 125 nm or 250 nm thick). The XUV beam transmitted through the sample was spectrally dispersed by a flat-field grating and projected on a XUV-sensitized camera[23]. Our measurements were performed near (to within $<$10%) optical breakdown. NIR-field-induced breakdown manifested itself as macroscopic mechanical damage of the sample, which became immediately visible in the magnified image of the focal region, which was permanently monitored.

NIR transmittivity and reflectivity. Field-induced changes in NIR transmittivity through 125-nm films and the reflectivity of thin ($\sim$0.2 mm) wedged plates were studied with laser pulses of less than 4 fs gently focused and the intensity on the sample was varied by translating it longitudinally along the optical axis (z-scan). The pump–probe measurement is sketched schematically in Fig. 3a. The incident NIR beam was split into two collinear beams by a two-component plane mirror consisting of a 5-mm-diameter inner section and a concentric external section. The inner and outer sections reflected the weak probe and the strong pump beam with a reflectivity of 10% and 97.5%, respectively. The energy of the pump pulse was controlled by an aperture. The probe pulse was delayed by translating the inner section with a piezo stage and focused along with the pump pulse onto the sample. The probe beam was isolated with an iris in front of the detector measuring the reflected probe pulse energy as a function of pump–probe delay. A more detailed description of the Methods is given in the Supplementary Information.

Received 20 December 2011; accepted 24 October 2012.
Published online 5 December 2012.

1. Zener, C. A theory of the electrical breakdown of solid dielectrics. *Proc. R. Soc. Lond. A* **145,** 523–529 (1934).
2. Wannier, G. Wave functions and effective Hamiltonian for Bloch electrons in an electric field. *Phys. Rev.* **117,** 432–439 (1960).
3. Franz, W. Einfluß eines elektrischen Feldes auf eine optische Absorptionskante. *Z. Naturforsch. A* **13,** 484 (1958).
4. Keldysh, L. V. Behavior of non-metallic crystals in strong electric fields. *Sov. J. Exp. Theor. Phys.* **6,** 763 (1958).
5. Mizumoto, Y., Kayanuma, Y., Srivastava, A., Kono, J. & Chin, A. H. Dressed-band theory for semiconductors in a high-intensity infrared laser field. *Phys. Rev. B* **74,** 045216 (2006).
6. Lenzner, M. *et al.* Femtosecond optical breakdown in dielectrics. *Phys. Rev. Lett.* **80,** 4076–4079 (1998).
7. Gertsvolf, M., Spanner, M., Rayner, D. M. & Corkum, P. B. Demonstration of attosecond ionization dynamics inside transparent solids. *J. Phys. At. Mol. Opt. Phys.* **43,** 131002 (2010).
8. Mitrofanov, A. *et al.* Optical detection of attosecond ionization induced by a few-cycle laser field in a transparent dielectric material. *Phys. Rev. Lett.* **106,** 147401 (2011).
9. Shih, T., Winkler, M. T., Voss, T. & Mazur, E. Dielectric function dynamics during femtosecond laser excitation of bulk ZnO. *Appl. Phys. A* **96,** 363–367 (2009).
10. Ghimire, S. *et al.* Redshift in the optical absorption of ZnO single crystals in the presence of an intense midinfrared laser field. *Phys. Rev. Lett.* **107,** 167407 (2011).
11. Ghimire, S. *et al.* Observation of high-order harmonic generation in a bulk crystal. *Nature Phys.* **7,** 138 (2011).
12. Durach, M., Rusina, A., Kling, M. & Stockman, M. Metallization of nanofilms in strong adiabatic electric fields. *Phys. Rev. Lett.* **105,** 086803 (2010).
13. Durach, M., Rusina, A., Kling, M. & Stockman, M. Predicted ultrafast dynamic metallization of dielectric nanofilms by strong single-cycle optical fields. *Phys. Rev. Lett.* **107,** 086602 (2011).
14. Schiffrin, A. *et al.* Optical-field-induced current in dielectrics. *Nature* doi:10.1038/nature11567 (this issue).
15. Goulielmakis, E. *et al.* Real-time observation of valence electron motion. *Nature* **466,** 739–743 (2010).
16. Kienberger, R. *et al.* Atomic transient recorder. *Nature* **427,** 817–821 (2004).
17. Bloch, F. Über die Quantenmechanik der Elektronen in Kristallgittern. *Z. Phys.* **52,** 555–600 (1929).
18. Wannier, G. H. *Elements of Solid State Theory. Elements* 173–177 (Cambridge Univ. Press, 1959).
19. Bleuse, J., Bastard, G. & Voisin, P. Electric-field-induced localization and oscillatory electro-optical properties of semiconductor superlattices. *Phys. Rev. Lett.* **60,** 220–223 (1988).
20. Mendez, E., Agulló-Rueda, F. & Hong, J. Stark localization in GaAs-GaAlAs superlattices under an electric field. *Phys. Rev. Lett.* **60,** 2426–2429 (1988).
21. Mendez, E. E. & Bastard, G. Wannier-Stark ladders and Bloch oscillations in superlattices. *Phys. Today* **46,** 34, http://dx.doi.org/10.1063/1.881353 (1993).
22. Fiess, M. *et al.* Versatile apparatus for attosecond metrology and spectroscopy. *Rev. Sci. Instrum.* **81,** 093103 (2010).
23. Schultze, M. *et al.* State-of-the-art attosecond metrology. *J. Electron Spectrosc. Relat. Phenom.* **184,** 68–77 (2011).
24. Li, D. *et al.* X-ray absorption spectroscopy of silicon dioxide (SiO_2) polymorphs; the structural characterization of opal. *Am. Mineral.* **79,** 622–632 (1994).

Supplementary Information is available in the online version of the paper.

Acknowledgements This work was supported by the Max Planck Society and the Deutsche Forschungsgemeinschaft Cluster of Excellence: Munich Centre for Advanced Photonics (www.munich-photonics.de).The work of M.I.S. and V.A. was supported by grant number DEFG02-01ER15213 from the Chemical Sciences, Biosciences and Geosciences Division and by grant number DE-FG02-11ER46789 from the Materials Sciences and Engineering Division of the Office of the Basic Energy Sciences, Office of Science, US Department of Energy. We thank K. Yabana, R. Ernstorfer and N. Karpowicz for discussions.

Author Contributions M.S., R.K., M.I.S. and F.K. conceived and supervised the study. M.S., E.M.B., A.S., S.H., W.S., M.F. and M.H. prepared and performed the experiment. V.A. and M.I.S. accomplished the theoretical modelling. M.S., E.M.B., A.S., V.S.Y. and F.K. analysed and interpreted the experimental data. All authors discussed the results and contributed to the final manuscript.

Author Information Reprints and permissions information is available at www.nature.com/reprints. The authors declare no competing financial interests. Readers are welcome to comment on the online version of the paper. Correspondence and requests for materials should be addressed to M.S. (martin.schultze@mpq.mpg.de), M.I.S. (mstockman@gsu.edu) and F.K. (krausz@lmu.de).